Systemic venous circulation. Waves propagating on a windkessel: relation of arterial and venous windkessels to systemic vascular resistance

Jiun-Jr Wang, Jacqueline A. Flewitt, Nigel G. Shrive, Kim H. Parker and John V. Tyberg

You might find this additional information useful...

This article cites 25 articles, 20 of which you can access free at:
http://ajpheart.physiology.org/cgi/content/full/290/1/H154#BIBL

Updated information and services including high-resolution figures, can be found at:
http://ajpheart.physiology.org/cgi/content/full/290/1/H154

Additional material and information about *AJP - Heart and Circulatory Physiology* can be found at:
http://www.the-aps.org/publications/ajpheart

This information is current as of January 3, 2007 .

Systemic venous circulation. Waves propagating on a windkessel: relation of arterial and venous windkessels to systemic vascular resistance

Jiun-Jr Wang,[1] Jacqueline A. Flewitt,[1] Nigel G. Shrive,[1] Kim H. Parker,[2] and John V. Tyberg[1]

[1]*Cardiovascular Research Group, Departments of Cardiac Sciences, Physiology and Biophysics, and Civil Engineering, University of Calgary, Calgary, Canada; and* [2]*Department of Bioengineering, Imperial College of Science, Technology and Medicine, London, United Kingdom*

Wang, Jiun-Jr, Jacqueline A. Flewitt, Nigel G. Shrive, Kim H. Parker, and John V. Tyberg. Systemic venous circulation. Waves propagating on a windkessel: relation of arterial and venous windkessels to systemic vascular resistance. *Am J Physiol Heart Circ Physiol* 290: H154–H162, 2006. First published August 19, 2005; doi:10.1152/ajpheart.00494.2005.—Compared with arterial hemodynamics, there has been relatively little study of venous hemodynamics. We propose that the venous system behaves just like the arterial system: waves propagate on a time-varying reservoir, the windkessel, which functions as the reverse of the arterial windkessel. During later diastole, pressure increases exponentially to approach an asymptotic value as inflow continues in the absence of outflow. Our study in eight open-chest dogs showed that windkessel-related arterial resistance was ~62% of total systemic vascular resistance, whereas windkessel-related venous resistance was only ~7%. Total venous compliance was found to be 21 times larger than arterial compliance ($n = 3$). Inferior vena caval compliance (0.32 ± 0.015 ml·mmHg^{-1}·kg^{-1}; mean $\pm$ SE) was ~14 times the aortic compliance (0.023 ± 0.002 ml·mmHg^{-1}·kg^{-1}; $n = 8$). Despite greater venous compliance, the variation in venous windkessel volume (i.e., compliance × windkessel pulse pressure; 7.8 ± 1.1 ml) was only ~32% of the variation in aortic windkessel volume (24.3 ± 2.9 ml) because of the larger arterial pressure variation. In addition, and contrary to previous understanding, waves generated by the right heart propagated upstream as far as the femoral vein, but excellent proportionality between the excess pressure and venous outflow suggests that no reflected waves returned to the right atrium. Thus the venous windkessel model not only successfully accounts for variations in the venous pressure and flow waveforms but also, in combination with the arterial windkessel, provides a coherent view of the systemic circulation.

systemic circulation

SIGNIFICANT EFFORTS have been devoted to the understanding of arterial hemodynamics, but much less attention has been paid to the venous systems (3, 24). The application of frequency-domain impedance analysis to venous pressure and flow seemed less successful than to arterial pressure and flow because the apparent reflection site was difficult to explain physiologically (27, 32). Brecher studied venous hemodynamics, and Sjostrand suggested that the cavae constituted a "surge chamber," which Rushmer termed a "preventricular sump." Noordergraaf (24) concluded that "no analytical treatment of the pressure-flow relationship in relation to. . .cardiac activity has been proposed. As a consequence, Brecher's suggestion that the central veins constitute the functional counterpart of the arterial reservoir, transforming steady flow into pulsatile flow, has not received the scientific scrutiny that such an intuitively appealing idea deserves." Thus we have endeavored to develop a new model in an attempt to follow Brecher's suggestion and to understand venous hemodynamics better.

In 1992, Tyberg (33) proposed a steady-state hydraulic model in which the volumes of the arterial and venous reservoirs were functions of mean arterial and venous pressures, via their respective compliances; this model was used to describe the translocation of blood volume in terms of parallel shifts in venous pressure-volume relationships. Recently, the concept of a constant-pressure arterial reservoir was extended to the time-varying state in which the arterial windkessel discharges during diastole, to be recharged during the subsequent systole (35). We now propose that the venous system is characterized by an analogous windkessel behavior: during the later part of diastole, pressure rises exponentially to approach an asymptotic value as inflow continues while venous outflow is negligible. In addition, waves propagate on this time-varying reservoir, the venous windkessel.

We first calculated the pressure change due (via venous compliance) to the volume change in the venous reservoir. By integrating this rate of pressure change, we obtained the windkessel pressure (P_{Wk}) over the cardiac cycle. We defined the difference between pressure in the inferior vena cava (P_{IVC}) and P_{Wk} as the excess pressure (P_{ex}), the pressure due to waves (17, 35). We then compared P_{ex} with the measured outflow (Q_{IVC}). Our finding that P_{ex} is proportional to Q_{IVC} suggests that waves generated by the right atrium (RA) and right ventricle (RV) account for the temporal variation in Q_{IVC}.

METHODS

Glossary

C_a	Arterial compliance (ml·mmHg^{-1}·kg^{-1})
IVC	inferior vena cava
C_{IVC}	IVC compliance (ml·mmHg^{-1}·kg^{-1})
P_a	Arterial pressure (mmHg)
P_{ex}	Excess pressure (mmHg)
P_{IVC}	IVC pressure (mmHg)
P_{Wk}	Windkessel pressure (mmHg)
P_∞	Asymptotic pressure (mmHg)
P_{RVED}	RV end-diastolic pressure (mmHg)
Q_a	Arterial flow (l/min)
Q_{IVC}	IVC flow (l/min)
$R_{large\ arteries}$	Large-artery resistance (mmHg·min·l^{-1})

$R_{large\ veins}$	Large-vein resistance (mmHg·min·l^{-1})
R_{Wk-a}	Arterial windkessel resistance (mmHg·min·l^{-1})
R_{Wk-IVC}	IVC windkessel resistance (mmHg·min·l^{-1})
SVR	Systemic vascular resistance (mmHg·min·l^{-1})
V_{Wk}	Venous reservoir volume (ml)
ΔV_{Wk-a}	Pulse volume variation in arterial windkessel (ml)
ΔV_{Wk-IVC}	Pulse volume variation in IVC windkessel (ml)
τ	Time constant of exponential rise in diastolic P_{IVC} (s)

Venous windkessel theory. The change in venous reservoir pressure, P_{Wk}, was assumed proportional to the change in the venous reservoir volume (i.e., V_{Wk}), which in turn, is the difference between inflow and outflow,

$$\frac{dP_{Wk}(t)}{dt} = \frac{1}{C}\frac{dV_{Wk}(t)}{dt} = \frac{Q_{in}(t) - Q_{out}(t)}{C} \quad (1)$$

where $C = dV_{Wk}/dP_{Wk}$ and is the compliance of the whole IVC system, which was assumed to be constant. IVC outflow (Q_{out}) was measured just proximal to the RA. The inflow (Q_{in}) was assumed to be driven by the gradient between the asymptotic pressure (P_∞, toward which P_{IVC} exponentially rises during diastole) and the venous reservoir pressure (P_{Wk}), across a resistance (R), or in mathematical form, $Q_{in}(t) = [P_\infty - P_{Wk}(t)]/R$.

By substituting Q_{in} in terms of P_{Wk} and P_∞, *Eq. 1* can be rewritten in terms of the windkessel pressure, P_{Wk}, as

$$\frac{dP_{Wk}(t)}{dt} + \frac{P_{Wk}(t) - P_\infty}{RC} = -\frac{Q_{out}(t)}{C}, \quad (2)$$

the general solution of which is

$$P_{Wk}(t - t_0) = P_\infty + (P_0 - P_\infty)e^{\frac{-(t-t_0)}{RC}} - e^{\frac{-(t-t_0)}{RC}}\int_{t_0}^{t}\frac{Q_{out}(t')}{C}e^{\frac{t'}{RC}}dt', \quad (3)$$

in which t_0 and P_0 are the time and pressure at the beginning of the cycle (defined as the onset of RA contraction), respectively. The time constant, $\tau = R \times C$, characterizes the exponential rise of P_{IVC}.

To solve *Eq. 3*, we had to determine R, C, and P_∞ using experimental data. Because Q_{IVC} is minimal during late diastole and because there is no significant wave motion, the observed exponential rise in P_{IVC} can be attributed to the charging of the venous system by inflow. Therefore, P_{IVC} approximates P_{Wk} during this time.

P_∞ was initially determined by fitting P_{IVC} data during the later part of diastole (when venous outflow is minimal; see the vertical dashed lines, Fig. 1) using a three-parameter exponential-rise equation. With arbitrary initial guesses for R and C (5 mmHg·min·l^{-1} and 2 ml/mmHg, respectively), they can be determined using a nonlinear search algorithm to minimize the mean-squared error between the calculated P_{Wk} and the measured P_{IVC}. The minimization was done using the Matlab (Mathworks, Natick, MA) routine "fminsearch," which uses the Nelder-Mead simplex (direct search) method. Many combinations of R and C yield the same τ, but only very narrow sets of values yield a P_{Wk} that relates to P_{IVC} appropriately, throughout the entire cardiac cycle. The calculation is not restricted to one cardiac cycle; it can be extended to multiple cycles. The difference between P_{IVC} and P_{Wk} is defined as excess pressure (i.e., the pressure due to waves): $P_{ex} = P_{IVC} - P_{Wk}$ (35).

To compare the venous and the arterial systems, we calculated the arterial windkessel using the methods previously described (35). We then calculated the "pulse volume variations" of the respective windkessels, which were determined by the magnitude of the windkessel pressure multiplied by the compliance, $\Delta V_{Wk} = C \times \Delta P_{Wk}$.

Experimental preparation and protocol. The protocol for the animal experiments conformed to the "Guiding Principles of Research Involving Animals and Human Beings" of the American Physiological Society and was approved by the University of Calgary animal care committee.
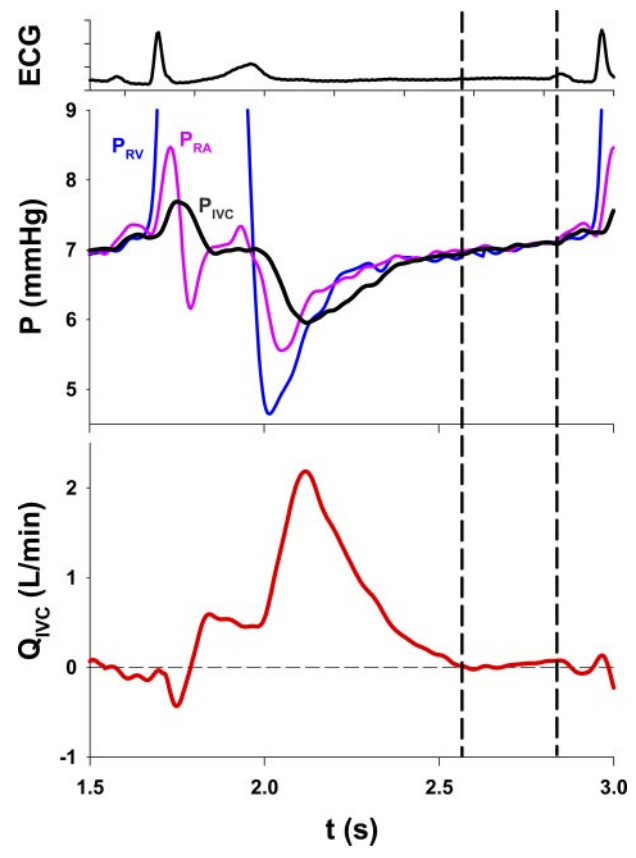

Fig. 1. Typical measurements of the ECG (*top*), the right ventricular pressure (P_{RV}; blue), right atrial pressure (P_{RA}; pink), and inferior vena cava (IVC) pressure (P_{IVC}, black) (*middle*), and the IVC flow (Q_{IVC}; *bottom*). The interval between the dashed lines, during which Q_{IVC} is minimal and P_{IVC} rises exponentially, was used for the calculation of windkessel pressure. *t*, Time.

Experiments were performed on eight healthy mongrel dogs weighing between 16 and 30 kg. Dogs were anesthetized with thiopental sodium (20 mg/kg) followed by fentanyl citrate (30 µg·kg^{-1}·h^{-1}) and ventilated with a 1:1 nitrous oxide-oxygen mixture. The rate of a constant-volume respirator (model 607; Harvard Apparatus, Natick, MA; tidal volume = 15 ml/kg) was adjusted to maintain normal blood gas tensions and pH. Body temperature was maintained at 37°C with the use of a circulating-water warming blanket and a heating lamp. A 10% pentastarch solution (Pentaspan; Bristol-Myers Squibb Canada, Montreal, Quebec, Canada) was infused to increase RV end-diastolic pressure (P_{RVED}).

Pressures were measured using high-fidelity catheter-tip manometers (Millar Instruments, Houston, TX) referenced to pressures measured externally (Statham-Gould, Oxnard, CA) via liquid-filled lumens and zeroed to the height of the RA. Flows were measured using an ultrasonic flowmeter (Transonic Systems, Ithaca, NY). We measured RV pressure (P_{RV}) by inserting a manometer through the RV apex and RA pressure (P_{RA}) by inserting a micromanometer (2F; Millar) through the RA appendage. Simultaneous pressures and flows were measured in the IVC (no more than 2 cm from the RA) and in the aortic root. In three dogs, pressure and flow also were measured in the superior vena cava (SVC). In the other five dogs, two additional flow probes were positioned, one just downstream to the renal veins and the other at the bifurcation, to measure simultaneous pressure and flow during pull back (see below). The IVC manometer was inserted through a femoral vein and the SVC manometer through a jugular vein. The aortic manometer was inserted through a femoral artery. The second jugular vein was cannulated for volume loading. To control the heart rate during the pull-back measurements, we paced

the RA via epicardial electrodes by using a laboratory stimulator (model S88; Grass Instrument, Quincy, MA). All data were recorded after the respirator had been turned off at end expiration.

After the control recordings were obtained (P_{RVED} ~3 mmHg), P_{RVED} was raised to ~5, ~10, and then ~15 mmHg. At $P_{RVED} \approx 10$ mmHg, the heart was paced at the lowest possible rate [zatebradine (ULFS 49)], and the IVC manometer was pulled back by 2-cm increments to the femoral vein, with pressures recorded at each position with the ventilator turned off at end expiration. Three-dimensional plots of venous pressure versus time and distance from the RA were constructed, using the ECG as a temporal reference. Distal venous flows were related to simultaneously measured pressures. The IVC manometer was repositioned back to within 2 cm of the RA before P_{RVED} was increased to 15 mmHg. At the end of the volume loading, a bolus of acetylcholine (~10 mg) was injected into the RA to produce a long (4–10 s) diastolic pause.

RESULTS

In Fig. 2, we show the behavior of the IVC hydraulic integrator when a long cardiac cycle was induced by an injection of acetylcholine. The simultaneously measured P_{RV} and P_{IVC} values and the calculated P_{Wk} and P_∞ values are shown in Fig. 2, *top*. The measured outflow, Q_{IVC}, the calculated inflow, Q_{in}, and the calculated excess pressure, P_{ex}, are shown in Fig. 2, *bottom*. (To compare the contours of P_{ex} and Q_{IVC}, we reversed the sign of P_{ex} and adjusted the scale so that their peak values coincided.) When Q_{in} equals Q_{IVC} (indicated by the vertical dashed lines), there is no change in P_{Wk}. During diastole, $Q_{in} > Q_{IVC}$ and P_{Wk} increases as the reservoir
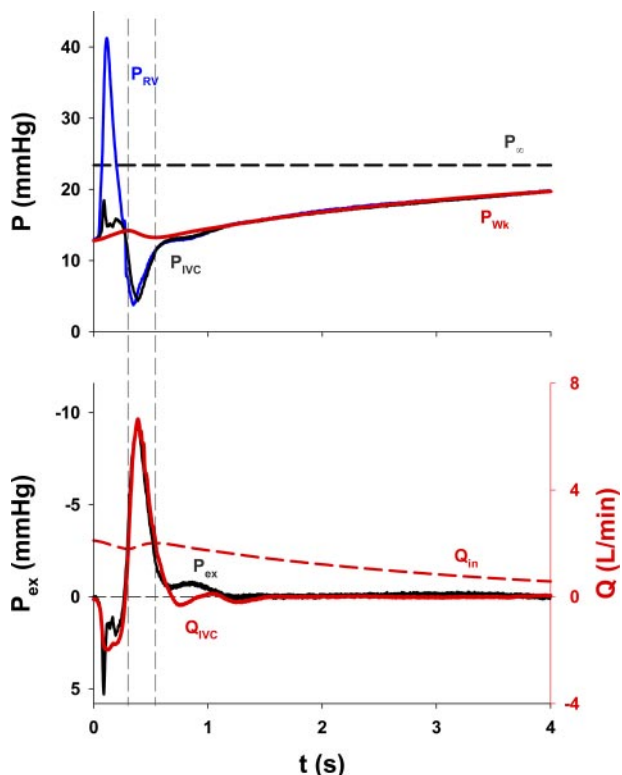

Fig. 2. A long cardiac cycle induced by the injection of acetylcholine. *Top*: measured P_{RV} (blue) and P_{IVC} (black) and calculated windkessel pressure (P_{Wk}; red) and asymptotic pressure (P_∞; black dashed line). *Bottom*: measured Q_{IVC} and calculated inflow (Q_{in}). Calculated excess pressure (P_{ex}) is proportional to Q_{IVC}. Vertical dashed lines indicate the instants at which $Q_{in} = Q_{IVC}$ where, therefore, P_{Wk} does not change.
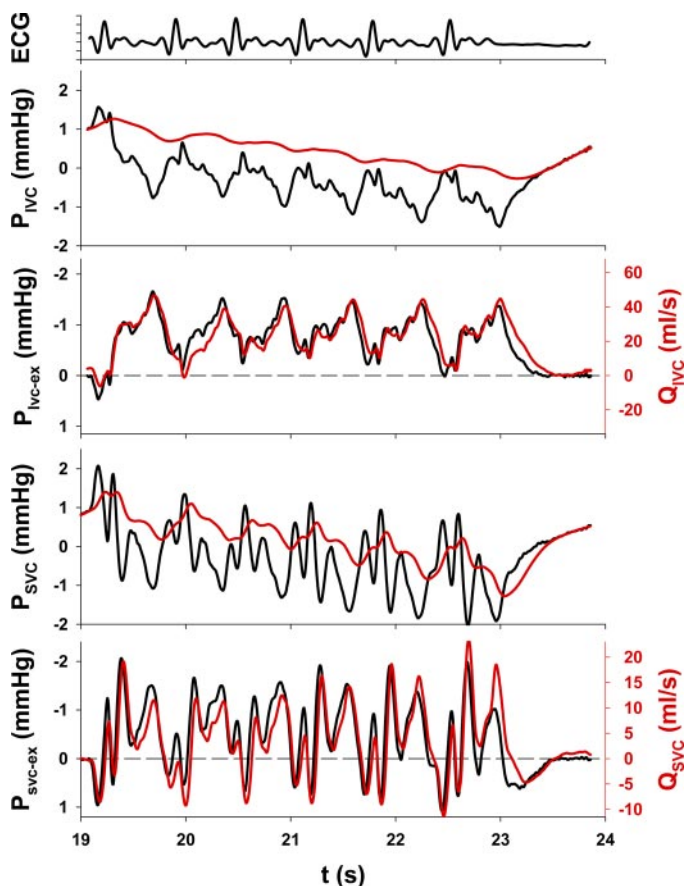

Fig. 3. Sinus arrhythmia. *Top* to *bottom*: ECG; measured P_{IVC} (black) and calculated $P_{Wk\text{-}IVC}$ (red); calculated $P_{IVC\text{-}ex}$ (black) and measured Q_{IVC} (red); measured superior vena cava (SVC) pressure (P_{SVC}; black) and calculated $P_{Wk\text{-}SVC}$ (red); and calculated $P_{SVC\text{-}ex}$ (black) and measured SVC flow (Q_{SVC}). For both IVC and SVC cases, P_{ex} and Q are respectively proportional. Note the different scales (Q_{IVC} vs. Q_{SVC}).

(windkessel) is charged by Q_{in} from the arterial circulation. Q_{in} is regulated by a venous peripheral resistance, R_{Wk}, and is driven by the gradient between P_∞ and P_{Wk}. The charging of the reservoir would cease when P_{IVC} reached the level of P_∞. The pressure due to waves, which was characterized by P_{ex}, the difference between the measured P_{IVC} and P_{Wk}, is precisely proportional to Q_{IVC} (*bottom*). The proportionality factor (P_{ex}/Q_{IVC}), which we interpret as the resistance of the large veins, is numerically equal to the characteristic impedance of the IVC (35).

The simultaneously measured IVC and SVC pressure and flow values and the calculated P_{Wk} and P_{ex} values during an interval of sinus arrhythmia are shown in Fig. 3. P_∞, *R*, and C were determined for the IVC and SVC by using the long diastole of the last beat, and each set of parameters was applied to calculate $P_{Wk\text{-}IVC}$ and $P_{Wk\text{-}SVC}$ during the whole series of beats. Note that the variation in P_{IVC} was slightly less than that of P_{SVC} but that the variation in Q_{IVC} was approximately threefold greater than that in Q_{SVC}.

In Fig. 4, *top*, P_{IVC} is plotted against time and distance at $P_{RVED} \approx 10$ mmHg. Waves, corresponding to the maxima and minima in P_{RA}, propagated through the IVC as far as measurements were made (i.e., to the femoral vein). However, during the later part of diastole, no wave motion was apparent and pressure increased uniformly and simultaneously throughout
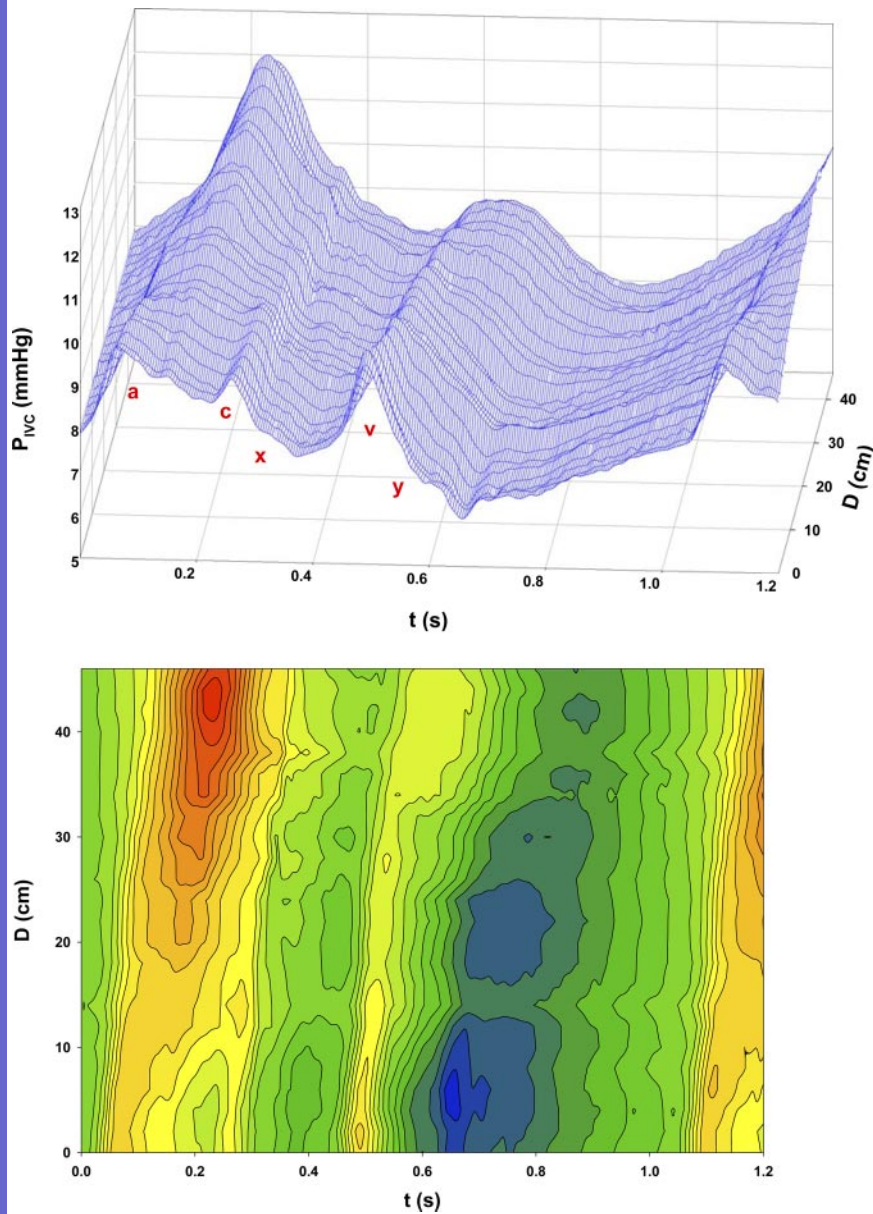
Fig. 4. *Top*: P_{IVC} plotted against time and distance (D) from the right atrium (RA) to the femoral vein. *Bottom*: corresponding contour plot of P_{IVC}, where the highest pressures are indicated in red and the lowest in blue. Isobar increment = 0.2 mmHg.

the length of the venous system. This uniformity can be best appreciated from the contour plot (Fig. 4, *bottom*; isobar increment = 0.2 mmHg) between ~0.85 and 1.05 s.

In Fig. 5, we show the simultaneous IVC pressure and flow values measured at three locations: just adjacent to the RA, just upstream from the renal veins (~18 cm to the RA), and further upstream at the bifurcation (~30 cm from the RA). At sites progressively further upstream, the variation of flow diminished but the variation of pressure was relatively unchanged. To observe wave propagation, on each pair of pressure flow panels we marked the beginning of the c wave and the beginning of the y descent with vertical lines. It took ~44 ms for these waves to travel from the RA to the renal veins and another 27 ms to reach the bifurcation, corresponding to averaged wave speeds of 4.1 m/s between the RA and renal veins and 4.4 m/s between the renal veins and the bifurcation.

C_{IVC} was plotted versus mean P_{IVC} for individual dogs, each at three levels of volume loading (Fig. 6). No pressure dependence was demonstrated.

DISCUSSION

Within the broad context of cardiovascular investigation, the study of venous hemodynamics has never received much emphasis, at least compared with the extensive studies of the heart and the many studies of the arterial circulation. The challenge to complete the systemic circulation with a conceptually coherent paradigm has remained formidable. No explanation for the variation in venous pressure and flow waveforms has yet been provided in that the few attempts by impedance analysis failed to relate plausibly the putative reflection sites to anatomical structures (27, 32). Despite the classical 1913 observations of MacKenzie (20) on jugular venous pulsations, controversy persisted whether pulsatile waveforms could be
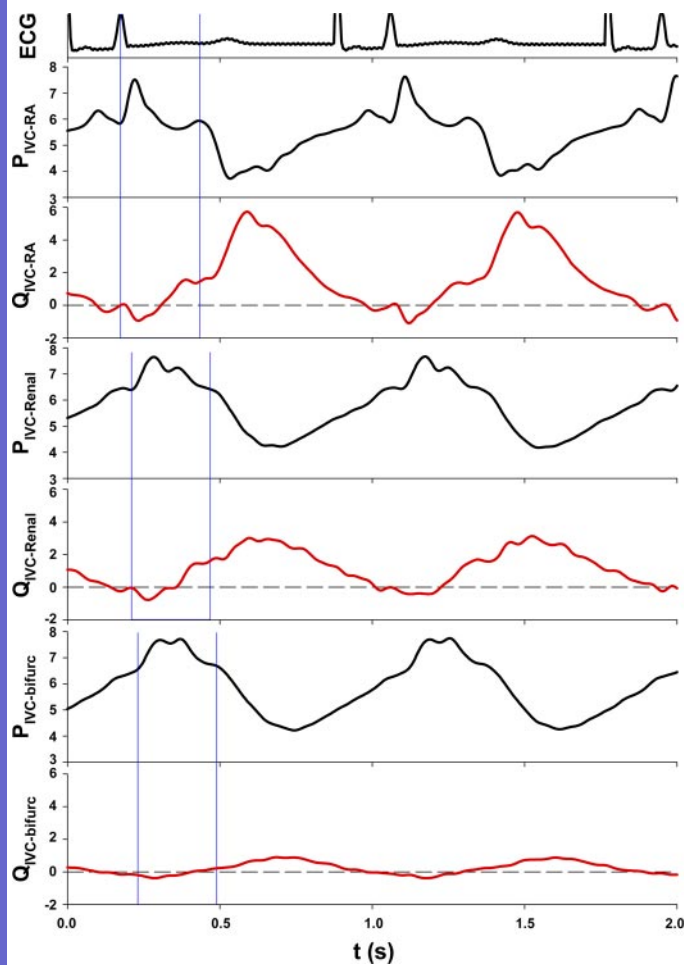
Fig. 5. Simultaneously measured IVC pressure and flow at 3 locations. *Top* to *bottom*: ECG (pacing spike is off scale); pressure (P_{IVC-RA}; mmHg) and flow (Q_{IVC-RA}; ml/s) measurements just adjacent to the RA; pressure ($P_{IVC-Renal}$) and flow ($Q_{IVC-Renal}$) measurements just downstream from the renal veins ($\sim$18 cm from the RA); and pressure ($P_{IVC-bifurc}$) and flow ($Q_{IVC-bifurc}$) measurements at the bifurcation ($\sim$30 cm from the RA). To define wave propagation, we marked the beginning of the *c* wave and the beginning of the *y* descent with vertical lines on each pair of panels.

emphasized the principle that the heart can only pump the blood that returns from the venous system, the narrow focus on this segment of the total circulation arguably overemphasized the resistance of the venules and veins, which together compose only $\sim$10% (7) of the total resistance between the aorta and the RA (Guyton related distributed total blood volume to cardiac output, which required that he weight the arterial and venous resistances according to their respective capacitances), and underemphasized those elements of the circulation that continually refill the reservoirs that are the source of venous return. Thus, in our view, his interpretation did not provide complete balance with respect to the circulation as a whole. This paradigm reduced to a system in which P_{RA}, "the back pressure to venous return," determined venous return and became the independent variable.

In 1979, Levy (16) reported the results of an experiment that was fundamentally similar to Guyton's and proposed an alternative paradigm in which cardiac output was the independent variable. Both Guyton and Levy emphasized the inverse relationship between cardiac output (equal to venous return in the steady state) and venous or RA pressure. However, from Levy's perspective, increasing the cardiac output augmented the arterial reservoir and depleted the venous reservoir and, therefore, caused venous pressure to decrease. In 1992, on the basis of the pressure-volume relationships of the arteries and the veins, Tyberg extended Levy's model and represented the peripheral systemic circulation as a high-pressure, low-compliance arterial reservoir functionally separated from a low-pressure, high-compliance venous reservoir by a lumped systemic vascular resistance (33). Our present conception of the arterial and the venous systems is, in fact, an extension of that steady-state, mean-pressure hydraulic reservoir model to a dynamic model in which arterial and venous windkessel pressures vary during the cardiac cycle in precise proportion to the volumes that they contain. During later diastole, the arterial reservoir discharges and the venous reservoir charges; during systole, the arterial reservoir charges and, during early diastole, the venous reservoir discharges. [A century ago, Otto Frank used the term "windkessel," a term first appearing in a German translation of Hales's *Haemostatics* (22), to describe the

observed in the lower body. Brecher (3) believed that the venous flow is steady and laminar, except very close to the RA. Anliker et al. (2) induced high-frequency (20–100 Hz), small-amplitude sinusoidal changes in pressure in the canine common iliac vein and demonstrated substantial attenuation. However, it is not surprising to find high attenuation at high frequency, because dissipation is highly correlated with frequency and similar phenomena have been observed under many other circumstances (17). As shown in Figs. 4 and 5, we consistently observed the propagation of venous waves as far as the femoral veins, and the same phenomenon also has been observed in human lower limbs (1, 23).

Overall, however, the study of venous physiology has been dominated by Guyton's paradigm (11). With the laudable intent of demonstrating an important role for peripheral circulatory factors in modulating cardiac output, he focused attention on "venous return," the flow of blood (from distributed arterial and venous reservoirs held at an equivalent mean circulatory pressure) that discharged through a "resistance to venous return" into the RA. Although this construct effectively
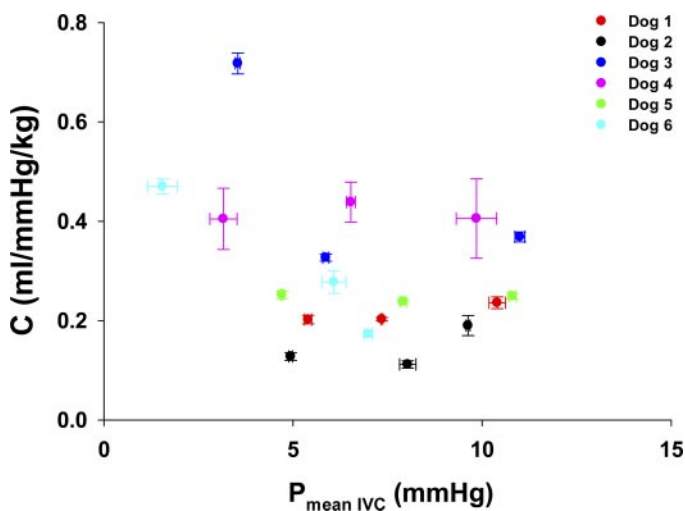

Fig. 6. IVC compliance (C) plotted vs. mean IVC pressure ($P_{mean\ IVC}$) during 3 stages of volume loading for individual dogs. Values are means $\pm$ SE.

change in pressure associated with the dynamic variations in reservoir volume (9, 29).]

We propose that the venous system behaves as waves propagating on a time-varying reservoir, the venous windkessel, which is the exact analog of our study of the arterial windkessel (35) but with reversed functionality. The analysis is simple and straightforward in principle. We first quantify the windkessel pressure by observing that, after the diastolic E wave and before the A wave (see Figs. 1 and 2), Q_{IVC} virtually stops and the gradient among the RV, RA, and IVC is negligible. Therefore, the calculated pressure associated with venous reservoir volume, P_{Wk}, should equal P_{IVC} during this period. The exponential rise of P_{IVC} is due to the charging of the venous reservoir by blood flowing into it from the arterial system. According to Lighthill (17; see also Ref. 35), the pressure associated with waves is the excess pressure, P_{ex}, which is the difference between the observed pressure (P_{IVC}) and the reservoir pressure (P_{Wk}). Under all experimental circumstances, P_{ex} was proportional to Q_{IVC}, which suggests that the variations in P_{ex} and Q_{IVC} could be completely accounted for by backward (i.e., upstream)-going waves and that no significant reflections were propagated back to the root of the IVC (35).

The strict proportionality between P_{ex} and Q_{IVC} over a wide range of P_{IVC} does imply that the irregular relationship between the venous pressure and flow can be simply explained by two "first-order" mechanisms: waves propagated upstream and volume variations due to windkessel charging and discharging. In the past, the irregular venous pressure and flow contours have only been considered to be the results of nonlinear effects, such as the effects of venous valves, muscle pumps (32), and/or partially collapsed vessels (27). However, the effects of venous valves and muscle pumps should have been minimal, because the animals in those studies were anesthetized in the supine position. There is a general perception that veins collapse to some degree, even with positive transmural pressure and with the animals in the supine position, where gravity plays a minor role (13). The collapsible tube phenomenon was first quantitatively described by Holt's bench-top experiment (14), which became the paradigm and was extensively studied using experimental (8, 15), mathematical (4, 15), and computational analysis (10, 25). However, all these previous studies were focused on large negative transmural pressures, and the results showed that nonlinear effects on pressure-flow relationship were insignificant if transmural pressure was positive or only slightly negative (4, 10, 25).

Our approach incorporates a three-element windkessel, but there are distinct differences between our time-domain approach and the impedance-analysis approach, and there may be theoretical and practical reasons why previous applications of impedance analysis failed to demonstrate three-element windkessel characteristics. In our view, the most important reason is theoretical and pertains to the fundamental conceptual difficulty associated with applying the logic of the arterial windkessel to the venous system. The venous windkessel is an upside-down version of the arterial windkessel, but the logic of this inversion is subtle. In addition, although the exponential behavior of the arterial windkessel may have been recognized, to our knowledge, a non-zero asymptotic pressure was never identified. For example, in developing their method to calculate arterial compliance, Yin et al. (18) used equations that are identical to ours except for the fact that they implicitly assumed that flow continued until arterial pressure equaled zero. Similarly, Guyton (12) and Sunagawa (34) devised circuits composed of a series of capacitors, all discharging to earth/ground level. According to our venous windkessel, venous pressure rises exponentially toward an asymptotic level and the flow into the venous windkessel is related to the inverse of the difference between this asymptotic pressure and venous (IVC) pressure. Zero pressure is completely irrelevant.

This problem is compounded by the fact that, with the conventional impedance analysis, mean values are subtracted out before the remaining periodic variations of pressure/flow are resolved into time-shifted sinusoidal components of variable magnitudes. Thus, even though the exponential nature of the equations and the electrical circuit might have been apparent, all absolute orientation (e.g., with respect to pressure in general and P_∞ in particular) is immediately lost.

However, all these problems notwithstanding, it is possible in retrospect to use Fourier analysis to define P_{ex} and P_{Wk}. Noting that our ratio P_{ex}/Q_{IVC} is equal to characteristic impedance (Z_0), one can multiply Z_0 by Q_{IVC} to get P_{ex} (26). P_{ex} then can be subtracted from P_{IVC} to yield P_{Wk}. Thus, once one appreciates that P_{IVC} is equal to the sum of P_{Wk} and P_{ex}, one can use Z_0 to duplicate our time-domain analysis.

An important practical reason for the difficulty in using impedance analysis is because it is severely limited in the absence of a steady state; the waveforms are not then truly periodic in the sense of being exactly reproducible and, if impedance analysis on single non-steady beats is attempted, spurious additional components have to be generated in each harmonic to accommodate the discontinuity. On the other hand, our approach is facilitated by the occasional appearance of longer diastolic periods during which Q_{IVC} is negligible.

Changing mean P_{IVC} (with volume loading) between ~2 and ~13 mmHg does not seem to change venous compliance significantly or consistently (Fig. 6). Although Magder (21) found that compliance decreased as pressure increased, at pressures less than 20 mmHg, no trend was clearly defined. Under control condition, IVC compliance averaged among eight dogs was 0.32 ± 0.02 ml·mmHg^{-1}·kg^{-1}, which is ~14 times of the arterial compliance (0.023 ± 0.002 ml·mmHg^{-1}·kg^{-1}; see Table 1). In the past, venous compliance has been studied using the two-port analysis: venous compliance ranged from 0.34 ± 0.11 to 1.25 ± 0.62 ml·mmHg^{-1}·kg^{-1}, depending on the manipulation of the baroreflex and infusion of norepinephrine (27).

Table 1. *IVC and aortic compliances and variation in windkessel volume*

	Windkessel Volume
Compliances, ml·mmHg^{-1}·kg^{-1}	
C_{IVC}	0.320 ± 0.015
C_a	0.023 ± 0.002
Variations, ml	
ΔV_{Wk-IVC}	7.8 ± 1.1
ΔV_{Wk-a}	24.3 ± 2.9

IVC, inferior vena cava; C_{IVC}, venous compliance; C_a, arterial compliance; ΔV_{Wk-IVC}, variation of the venous windkessel volume; ΔV_{Wk-a}, variation of the arterial windkessel volume. Values are means $\pm$ SE; $n = 8$.

In the three experiments in which we determined the parameters of the SVC, IVC, and aortic windkessels from simultaneously measured data, we found that the sum of the SVC and IVC (windkessel) compliances was an average of 21 times the compliance of the aortic windkessel. This compares very favorably with the value (i.e., 19 times) in Levy's model (16, 33).

Although the comparison of compliances is informative, a better index of their relative "size" may be a comparison of the volumes of blood that charge and discharge the windkessels during each cardiac cycle. This was obtained for the aorta and the IVC by taking the product of the respective windkessel pressure and compliance to obtain a "windkessel pulse volume" (i.e., the difference between the maximum and minimum windkessel volume). This analysis showed that the change in volume of the aortic windkessel was 3.33 ± 0.32 times the change in volume of the IVC windkessel. Even though the IVC compliance is much greater, the larger pressure variation in the aortic windkessel makes the aortic volume change substantially larger and, in a sense, more important physiologically.

Our studies of the arterial and venous windkessels have led us to modify our view of the peripheral systemic circulation. Consistent with previous ideas, in the language of an electrical analog, we suggest that a continuous resistor, the systemic vascular resistance (SVR), separates the potential levels corresponding to mean P_a and P_{IVC}. The extreme ends of this resistor represent large-artery and large-vein resistances and are mathematically equal to the respective ratios of P_{ex} to flow (i.e., P_{ex}/Q_a and P_{ex}/Q_{IVC}). [In turn, these ratios are quantitatively equal to arterial and venous characteristic impedance (35). It is interesting to note that Quick et al. (26) showed that the product of flow times characteristic impedance was equal to "reflectionless" pressure; we would say "windkessel-less" pressure, i.e., P_{ex}.] Segments of the resistor next to the large-artery and large-vein resistances are the resistances that define the time constants ($\tau = R \times C$) of the windkessels. (Compliances are well-defined physical vessel properties, but, to produce the observed time constants, they must be coupled with resistances.)

These concepts can be illustrated by considering order-of-magnitude values (Table 2 and Fig. 7; only the flow that returns to the heart via the IVC, $\sim$60% of aortic flow, is considered so that arterial parameters are scaled appropriately.) The value of the large-artery resistance is 3% of the total resistance, and the resistance of the arterial windkessel is 59%. The value of the
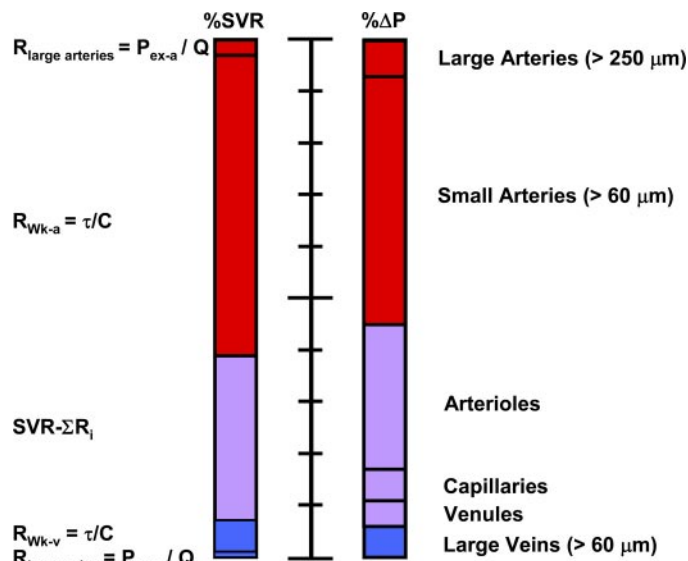

Fig. 7. Relation of arterial and venous windkessels to systemic vascular resistance (SVR) compared with the results of micropuncture measurements of vascular pressures in the hamster cheek pouch (7). Column at *left* indicates arterial and venous windkessel-related resistances, expressed as percentages of total SVR. Column at *right* indicates pressures of arterial and venous vessels, expressed as percentages of the total arteriovenous pressure drop (ΔP). Note that the arterial windkessel appears to involve large and small (>60 μm) arteries and the venous windkessel, "large" (>60 μm) veins. See text for detailed description and glossary for definitions.

large-vein resistance is 1%, and the resistance of the venous windkessel is 6%. By difference, this implies that the value of the remaining intermediate segment of the total systemic vascular resistance is 31%. This implies that the arterial windkessel extends downstream $\sim$60% of the extent of the equivalent series resistor (i.e., SVR) and that the venous windkessel extends upstream $\sim$7%.

It is interesting to compare these values to the direct measurements of mean pressure in the hamster cheek pouch preparation (7), because the fraction of the total proximal aorta-to-RA pressure drop is equivalent to the fraction of the total resistance (see Fig. 7). Davis et al. (7) found 55% of the pressure drop occurred across the large and small arteries (see their Fig. 8), 39% across the arterioles, capillaries, and venules, and 6% across large veins (i.e., > 60 μm). These comparisons imply that the arterial windkessel extends downstream into the microcirculation to include the small arteries (see red segments in Fig. 7) and that the venous windkessel extends upstream into the microcirculation to include veins > 60 μm (see blue segments in Fig. 7). Their value ($\sim$39%) for the microcirculation (i.e., arterioles, capillaries, and venules) is essentially equal to the residual resistance not accounted for by the arterial and venous windkessels (32%; purple segments in Fig. 7). Their values for large artery resistance ($\sim$7%) include arterial segments as small as 250 μm and, for large-vein resistance ($\sim$6%), venous segments as small as 60 μm. Thus our respectively smaller values for large artery and large-vein resistances (1.2 and 0.6%) would seem to correspond to the resistances of the larger of the "large" vessels, as they must if they represent the resistances of vessels interposed between the heart and the respective windkessels.

Our analysis might be better understood by considering Fig. 8, in which we compare incremental pressure differences to

Table 2. *Relation of arterial and venous windkessel-related resistances to SVR*

	Windkessel-Related Resistances	
	mmHg·min·l^{-1}	%
SVR	130.09 ± 28.70	100
$R_{\text{large arteries}}$	3.50 ± 0.40	2.96 ± 0.44
$R_{\text{Wk-a}}$	72.92 ± 13.88	58.82 ± 2.74
$R_{\text{Wk-v}}$	7.54 ± 1.59	5.98 ± 0.81
$R_{\text{large veins}}$	1.28 ± 0.48	0.97 ± 0.28
SVR-ΣR_i	45.15 ± 13.77	31.27 ± 2.68

SVR, systemic vascular resistance; $R_{\text{large arteries}}$, resistance of the large arteries; $R_{\text{Wk-a}}$, resistance of the arterial windkessel; $R_{\text{Wk-v}}$, resistance of the venous windkessel; $R_{\text{large veins}}$, resistance of the large veins; ΣR_i, sum of 4 windkessel-related resistances. Values are means $\pm$ SE; $n = 8$.
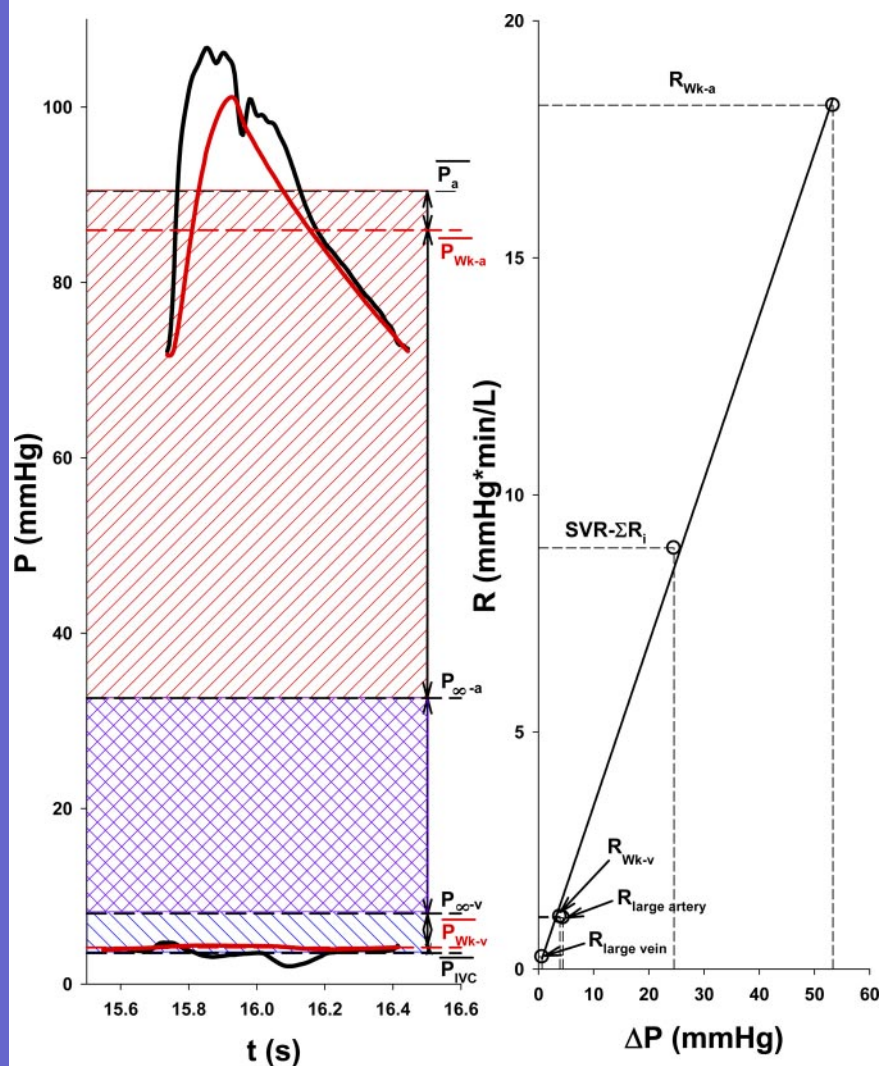
Fig. 8. Comparison of incremental pressure differences to calculated (as in Fig. 7) resistances for a representative cardiac cycle. At *left* are simultaneously measured arterial and IVC pressures (upper and lower black curves) and their calculated windkessel pressures (upper and lower red curves). The mean values of aortic ($\overline{P_a}$), arterial windkessel ($\overline{P_{Wk-a}}$), arterial asymptotic pressure ($\overline{P_{\infty-a}}$), IVC asymptotic pressure ($\overline{P_{\infty-v}}$), IVC windkessel pressure ($\overline{P_{Wk-v}}$), and IVC pressure ($\overline{P_{IVC}}$) are indicated by labeled horizontal dashed lines. The total arterial-venous pressure gradient was separated into arterial (red hatching; related to the large arteries and the arterial windkessel), microcirculatory (purple crosshatching), and venous (blue hatching; related to the large veins and the venous windkessel) sections, corresponding to Fig. 7. At *right*, the incremental resistances were plotted against the incremental pressure gradients (ΔP; corresponding to the vertical double-headed arrows at *left*).

calculated resistances (as in Fig. 7) for a representative cardiac cycle. First, the fact that mean aortic pressure is measurably higher than mean arterial windkessel pressure (the difference being related to P_{ex-a}) is entirely consistent with blood flowing through a large-artery resistance. Second, according to our theory (35), instantaneous flow out of the arterial windkessel is proportional to the difference between P_{Wk-a} and $P_{\infty-a}$, so the difference between mean P_{Wk-a} and $P_{\infty-a}$ should govern windkessel outflow during the cycle. The same is true of the venous system. The fact that mean IVC pressure is measurably lower than mean venous windkessel pressure (the difference being related to P_{ex-v}) is consistent with blood flowing through a large-vein resistance. Also, according to the theory given above, instantaneous flow into the venous windkessel is proportional to the difference between $P_{\infty-v}$ and P_{Wk-v}, and so the difference between mean $P_{\infty-v}$ and P_{Wk-v} should govern venous windkessel inflow during the cycle. Finally, we hold that the resistance between the arterial and venous windkessels (i.e., the microvascular resistance) should be a function of the difference between $P_{\infty-a}$ and $P_{\infty-v}$ (purple crosshatching in Fig. 8, *left*). As shown in Fig. 8, *right*, we compared these pressure differences to incremental resistances calculated from this

same beat and found an approximately linear relation, as expected ($r^2 = 0.998$).

In addition, Fig. 8 suggests a practical expedient that may prove useful. The fraction of total SVR accounted for by the microcirculatory resistance may vary widely, from ~40% (e.g., methoxamine) to ~15% (e.g., sodium nitroprusside) (unpublished data). As a first approximation, the resistance related to the venous windkessel (blue hatching in Fig. 8, *left*) might be ignored. The arterial diastolic data then could be fit to a simple, three-parameter exponential equation to estimate the value of $P_{\infty-a}$, which would indicate how much of the SVR is related to the arterial windkessel (red hatching) and how much to microcirculatory resistance (purple crosshatching). [This estimation might be difficult, practically, if the heart rate is high (i.e., >80 beats/min) but not with data from a longer cardiac cycle, as in the presence of normal sinus arrhythmia.]

The extents of the arterial and venous windkessels are defined by the values of their respective P_{∞} values. For the arterial system, these values correspond to "waterfall" (6, 19), Starling resistor (30, 31), or critical closing pressure (5) phenomena. Under our normal experimental conditions, $P_{\infty-a}$ is ~35 mmHg (35), but under the influence of methoxamine, this

value can approach 100 mmHg (unpublished observations). Also, under the influence of an acetylcholine injection that can produce a diastolic pause lasting 15–20 s, aortic pressure declines to ~15 mmHg, consistent with observations designed to estimate mean circulatory filling pressure (28). Finally, after death, the arterial-venous pressure gradient undoubtedly disappears. All these observations suggest that the value of $P_{\infty\text{-a}}$ is a function of the local biochemical, humoral, and mechanical milieu and that these factors can vary.

Limitations. In general, it is more difficult to determine windkessel parameters if the heart rate is fast ($>$70 beats/min). We view this as a practical but not a theoretical limitation. This difficulty can be minimized by selecting a sequence of beats that includes a longer diastole. (Since completion of the present experiments, we have found that momentary stimulation of the right vagus nerve prolongs diastole conveniently.) Because baroreceptor activity is known to affect the venous compliance (27), we allowed time between volume-loading interventions to achieve reequilibration.

In conclusion, we represent the venous circulation as a system in which waves propagate on a time-varying reservoir. This new model not only explains the details of the seemingly irregular IVC and SVC pressure and flow waveforms but also, in relation to systemic vascular resistance, provides a coherent view of the systemic circulation as a whole.

REFERENCES

1. **Abu-Yousef MM, Kakish ME, and Mufid M.** Pulsatile venous Doppler flow in lower limbs: highly indicative of elevated right atrium pressure. *Am J Roentgenol* 167: 977–980, 1996.
2. **Anliker M, Yates WG, and Ogden E.** Transmission of small pressure waves in the canine vena cava. *Am J Physiol* 221: 644–651, 1971.
3. **Brecher GA.** History of venous research. *IEEE Trans Biomed Eng* 16: 233–247, 1969.
4. **Brower RW and Noordergraaf A.** Pressure-flow characteristics of collapsible tubes: a reconciliation of seemingly contradictory results. *Ann Biomed Eng* 1: 333–355, 1973.
5. **Burton AC.** On the physical equilibrium of small blood vessels. *Am J Physiol* 164: 319–329, 1951.
6. **Caldini P, Permutt S, Waddell JA, and Riley RL.** Effect of epinephrine on pressure, flow, and volume relationships in the systemic circulation of dogs. *Circ Res* 34: 606–623, 1974.
7. **Davis MJ, Ferrer PN, and Gore RW.** Vascular anatomy and hydrostatic pressure profile in the hamster cheek pouch. *Am J Physiol Heart Circ Physiol* 250: H291–H303, 1986.
8. **Duomarco JL and Rimini R.** Energy and hydraulic gradients along systemic veins. *Am J Physiol* 178: 215–220, 1954.
9. **Frank O.** Die Grundform des Arteriellen Pulses. *Erste Abhandlung Mathematische Analyse Z Biol* 37: 483–526, 1899.
10. **Grotberg JB and Jensen OE.** Biofluid mechanics in flexible tube. *Annu Rev Fluid Mech* 36: 121–147, 2004.
11. **Guyton AC.** Determination of cardiac output by equating venous return curves with cardiac response curves. *Physiol Rev* 35: 123–129, 1955.
12. **Guyton AC and Coleman T.** *Circulatory Physiology: Cardiac Output and Its Regulation* (2nd ed.). Philadelphia, PA: Saunders, 1973, p. 255–262.
13. **Hargens AR, Millard RW, Pettersson K, and Johansen K.** Gravitational haemodynamics and oedema prevention in the giraffe. *Nature* 329: 59–60, 1987.
14. **Holt JP.** The collapse factor in the measurement of venous pressure: the flow of fluid through collapsible tubes. *Am J Physiol* 134: 292–299, 1941.
15. **Katz AI, Chen Y, and Moreno AH.** Flow through a collapsible tube. Experimental analysis and mathematical model. *Biophys J* 9: 1261–1279, 1969.
16. **Levy MN.** The cardiac and vascular factors that determine systemic blood flow. *Circ Res* 44: 739–747, 1979.
17. **Lighthill MJ.** *Waves in Fluids*. Cambridge: Cambridge University Press, 1978.
18. **Liu Z, Brin KP, and Yin FC.** Estimation of total arterial compliance: an improved method and evaluation of current methods. *Am J Physiol Heart Circ Physiol* 251: H588–H600, 1986.
19. **Lopez-Muniz R, Stephens NL, Bromberger-Barnea B, Permutt S, and Riley RL.** Critical closure of pulmonary vessels analyzed in terms of Starling resistor model. *J Appl Physiol* 24: 625–635, 1968.
20. **Mackenzie J.** *Diseases of the Heart*. London: Oxford University Press, 1913.
21. **Magder S.** Vascular mechanics of venous drainage in dog hindlimbs. *Am J Physiol Heart Circ Physiol* 259: H1789–H1795, 1990.
22. **Nichols WW and O'Rourke MF.** *McDonald's Blood Flow in Arteries*. New York: Arnold, 1998.
23. **Nippa JH, Alexander RH, and Folse R.** Pulse wave velocity in human veins. *J Appl Physiol* 30: 558–563, 1971.
24. **Noordergraaf A.** Veins. In: *Circulatory System Dynamics*. New York: Academic, 1978, p. 157–181.
25. **Pedley TJ and Luo XY.** Modeling flow and oscillations in collapsible tube. *Theoret Comput Fluid Dynamics* 10: 277–294, 1998.
26. **Quick CM, Berger DS, and Noordergraaf A.** Constructive and destructive addition of forward and reflected arterial pulse waves. *Am J Physiol Heart Circ Physiol* 280: H1519–H1527, 2001.
27. **Rose WC and Shoukas AA.** Two-port analysis of systemic venous and arterial impedances. *Am J Physiol Heart Circ Physiol* 265: H1577–H1587, 1993.
28. **Rothe CF.** Mean circulatory pressure: its meaning and measurement. *J Appl Physiol* 74: 499–509, 1993.
29. **Sagawa K, Lie RK, and Schaefer J.** Translation of Otto Frank's paper "Die Grundform des Arteriellen Pulses" Zeitschrift fur Biologie 37: 483–526 (1899). *J Mol Cell Cardiol* 22: 253–277, 1990.
30. **Shrier I and Magder S.** Response of arterial resistance and critical pressure to changes in perfusion pressure in canine hindlimb. *Am J Physiol Heart Circ Physiol* 265: H1939–H1945, 1993.
31. **Shrier I and Magder S.** Maximal vasodilation does not eliminate the vascular waterfall in the canine hindlimb. *J Appl Physiol* 79: 1531–1539, 1995.
32. **Sunagawa K, Harasawa Y, and Hayashida K.** Evaluation of dynamic mechanical characteristics of the systemic venous system by wide band high resolution impedance (Abstract). *Circulation* 74, *Suppl* II: II-440, 1986.
33. **Tyberg JV.** Venous modulation of ventricular preload. *Am Heart J* 123: 1098–1104, 1992.
34. **Uemura K, Sugimachi M, Kawada T, Kamiya A, Jin Y, Kashihara K, and Sunagawa K.** A novel framework of circulatory equilibrium. *Am J Physiol Heart Circ Physiol* 286: H2376–H2385, 2004.
35. **Wang JJ, O'Brien AB, Shrive NG, Parker KH, and Tyberg JV.** Time-domain representation of ventricular-arterial coupling as a windkessel and wave system. *Am J Physiol Heart Circ Physiol* 284: H1358–H1368, 2003.

American Journal of Physiology – Heart and Circulatory Physiology